Available online at www.sciencedirect.com
SCIENCE DIRECT®
Catalysis Today 90 (2004) 245–254
CATALYSIS TODAY
www.elsevier.com/locate/cattod

Defective structure, oxygen mobility, oxygen storage capacity, and redox properties of RE-based (RE = Ce, Pr) solid solutions

H. He [a,*], H.X. Dai [a], C.T. Au [b]

[a] *Environmental Catalysis Laboratory, Department of Applied Chemistry, College of Environmental and Energy Engineering, Beijing University of Technology, Beijing 100022, PR China*
[b] *Department of Chemistry, Hong Kong Baptist University, Kowloon Tong, Hong Kong*

Abstract

Defective structures, surface textures, oxygen mobility, oxygen storage capacity (OSC), and redox properties of $RE_{0.6}Zr_{0.4}O_2$ and of $RE_{0.6}Zr_{0.4-x}Y_xO_2$ (RE = Ce, Pr; $x = 0, 0.05$) solid solutions have been investigated using X-ray diffraction (XRD), temperature-programmed desorption (TPD), temperature-programmed reduction (TPR), O_2-H_2 and O_2-CO titration, $^{18}O/^{16}O$ isotope exchange, CO pulsing reaction, and X-ray photoelectron spectroscopy (XPS) techniques. The effects of doping noble metal onto $RE_{0.6}Zr_{0.4-x}Y_xO_2$ on oxygen mobility and surface oxygen activities have also been studied. Based on the experimental outcomes, we conclude that: (i) a Pr-based solid solution has better redox behavior than a Ce-based one; (ii) incorporation of yttrium ions in the lattices of CZ and PZ solid solutions could result in an enhancement in oxygen vacancy concentration, Ce^{4+}/Ce^{3+} and Pr^{4+}/Pr^{3+} redox properties, lattice oxygen mobility, and oxygen storage capacity; and (iii) doping the noble metal (Rh, Pt, and Pd) onto RE-based solid solution has positive effect on the properties concerned in this work.

Keywords: CeO_2-ZrO_2; PrO_2-ZrO_2; Redox property; Lattice oxygen mobility; Oxygen storage capacity; $^{18}O/^{16}O$ isotope exchange

1. Introduction

During the last decade, ceria-based solid solutions have been intensively studied for their utilization in three-way catalysts (TWCs) due to the multiple positive effects on the enhancement of catalytic performance. It is well known that the materials possess: (i) a large oxygen storage capacity (OSC) via a facile $Ce^{4+} \Leftrightarrow Ce^{3+}$ redox process; (ii) an ability of promoting dispersion of noble metals; and (iii) a promotional action to the water–gas-shift reaction. Among the properties of ceria-based solid solutions, the most important is related to its property of oxygen buffer. Ceria can release oxygen in fuel rich conditions and uptake it during lean fuel operation, guaranteeing a high elimination efficiency of three-way catalysts. In the past year, the oxygen storage capacity, redox properties, and utilization in TWCs of ceria-based solid solutions such as CeO_2–Al_2O_3, CeO_2–La_2O_3, CeO_2–SiO_2, CeO_2–HfO_2, and CeO_2–ZrO_2 have been intensively investigated [1–12]. Among them, CeO_2–ZrO_2 possesses the best thermal stability, excellent redox behavior, and high oxygen storage capacity. It has been recognized that redox behaviors and oxygen storage capacity of $Ce_{1-x}Zr_xO_2$ ($x = 0.1-0.9$) are related to both composition and structure of solid solution. Kašpar and co-workers [10,13] have showed that the $Ce_{0.5}Zr_{0.5}O_2$ displays an unusual improvement on redox behavior because of high oxygen mobility within the bulk after ZrO_2 doping. For optimum performance, Trovarelli et al. [14] and Hori et al. [15] concluded that the content of doped ZrO_2 should not exceed 50% for obtaining good redox property and high oxygen storage capacity. According to Madier et al. [16], $Ce_{0.63}Zr_{0.37}O_2$ is high in oxygen storage capacity and good in O_2 exchange reactivity.

Recently, many efforts have been focused on the investigation of defective structure, oxygen mobility, redox properties, effects on the oxygen storage capacity, and new fabrication methods of CeO_2–ZrO_2 solid solution [17–21]. According to the work reported by Yashima et al. [22], the two thermodynamically stable phase (*t*- and *c*-phase) were found in the $Ce_xZr_{1-x}O_2$ solid solutions, respectively, at high (0.80 mol%) and low (<20 mol%) ZrO_2 contents,

* Corresponding author. Tel.: +86-10-67396588; fax: +86-10-67391983.
E-mail address: hehong@bjpu.edu.cn (H. He).

0920-5861/$ – see front matter © 2004 Elsevier B.V. All rights reserved.
doi:10.1016/j.cattod.2004.04.033

while other two metastable tetragonal phase (t, t'') phases were detected at intermediate compositions. It was reported that the t'' phase of $Ce_xZr_{1-x}O_2$ solid solutions was responsible for good redox properties. Surface oxygen and oxygen vacancies are involved in catalytic activity, and enhanced oxygen mobility enable the occurrence of redox processes at lower temperatures.

The incorporation of Y^{3+}, La^{3+} or Ga^{3+} ions in the $Ce_{1-x}Zr_xO_2$ lattice facilitates the diffusion of oxygen by the formation of anion defects and decreases the temperature at which the redox process occurs [7,23,24].

We and other authors have reported that doping Y^{3+} ions into the lattice of CeO_2–ZrO_2 have a positive effect on its redox properties and oxygen storage capacity by creating oxygen vacancies inside the parent oxide [24].

PrO_2 are cubic fluorite-type in structure and can form solid solutions with other fluorite-type oxides as similar to CeO_2. Narula et al. [25] had investigated the oxygen storage capacities of single oxides (CeO_2, PrO_y, ZrO_2), binary oxides (CeO_2–ZrO_2, PrO_y–CeO_2, PrO_y–ZrO_2), and ternary oxides (PrO_y–CeO_2–ZrO_2), concluding that PrO_y–ZrO_2 shows the best oxygen storage capacity that increases non-linearly with PrO_y concentration. We contemplate that praseodymium-based solid solutions possess considerable potential to be another type of oxygen storage additives used in TWCs, which exhibit higher oxygen storage capacity and better redox properties than ceria-based solid solutions.In this work, the defective structures, surface textures, oxygen mobility, oxygen storage capacity, and redox properties of $RE_{0.6}Zr_{0.4}O_2$ and of $RE_{0.6}Zr_{0.4-x}Y_xO_2$ (RE = Ce, Pr; $x = 0$, 0.05) solid solutions have been investigated using X-ray diffraction (XRD), temperature-programmed reduction (TPR), temperature-programmed desorption (TPD), O_2–H_2 and O_2–CO titration, $^{18}O/^{16}O$ isotope exchange, CO pulsing reaction, and X-ray photoelectron spectroscopy (XPS) techniques. The effects of doping noble metal on $RE_{0.6}Zr_{0.4-x}Y_xO_2$ on oxygen mobility and surface oxygen activities have also been studied.

2. Experimental

The samples of $Ce_{0.6}Zr_{0.4}O_2$ (CZ), $Ce_{0.6}Zr_{0.35}Y_{0.05}O_2$ (CZY), $Pr_{0.60}Zr_{0.40}O_2$ (PZ), and $Pr_{0.60}Zr_{0.35}Y_{0.05}O_2$ (PZY) solid solutions were prepared by co-precipitation method from the corresponding chemicals: $Ce(NO_3)_3{\cdot}6H_2O$ (Aldrich, 99%), $ZrO(NO_3)_2{\cdot}xH_2O$ (Acros, 99.5%), Y_2O_3 (Acros, 99.99%; dissolved with HNO_3), and Pr_6O_{11} (Sigma, 99.9%; dissolved with HNO_3) at the appropriate ratios. The precursors were mixed in an aqueous solution, respectively, and then, an ammonia solution (3 N) was added dropwise to the solution to reach a pH value of ca. 10. The precipitates were washed with distilled water, filtered, dried at 80 °C overnight, and calcined at 550 °C in air for 5 h. The resulting powders were in turn ground, tabletted, crushed, and sieved to a size range of 60−80 mesh before use.

The Pd-, Pt-, Rh-loaded CZY and PZY catalysts (loading = 0.5 wt.%) were prepared by impregnating the CZY and PZY powders with $RhCl_3{\cdot}3H_2O$ (Acros, 33 wt.% Rh), $H_2PtCl_6{\cdot}6H_2O$ (Acros) and $PdCl_2$ (Acros, 59 wt.% Pd) solutions, respectively. Then the materials were dried at 80 °C overnight and then calcined at 550 °C for 5 h.

The TPR and TPD experiments were preformed in a quartz tubular micro-reactor. The sample (50 mg) was pretreated in a flow of 50% O_2−50% N_2 (v/v) (50 ml min^{-1}) at 500 °C for 1 h and then purged with N_2 at same temperature for 0.5 h, followed by cooling to room temperature, the temperature ramp rate in TPR is 10 °C min^{-1}. Before performing an O_2-TPD experiment, the sample was first pretreated in situ in O_2 (20 ml min^{-1}) at 450 °C for 1 h, followed by cooling to room temperature in the same atmosphere and purging with He (HKO, >99.995%, 20 ml min^{-1}) for 10 min. After being cooled to room temperature, the sample was heated from 30 to 900 °C at a rate of 10 °C min^{-1} for O_2 desorption. The flow rates of the 5% H_2−95% N_2 (v/v) mixture (for TPR) and He (for TPD) were 50 and 20 ml min^{-1}, respectively. The effluent gases were monitored on-line by a mass spectrometer (HP G-1800A) in TPD studies and a thermal conductivity detector in TPR investigations. The extent of O_2 desorption in TPD studies was quantified by calibrating peak area against that of a standard O_2 pulse. For the quantification of TPR profiles, the amount of H_2 consumption was calibrated against that consumed when a known quantity of CuO was reduced under a similar TPR condition.

For H_2–O_2 and CO−O_2 titrations, the experiments were performed in a quartz tubular micro-reactor (i.d. = 4 mm) by pulsing 50.0 μl O_2 and 50.0 μl H_2 (or CO), alternately, into the system. The sample (50 mg) was placed in the middle of the reactor secured by two quartz wool plugs. A thermocouple located at the catalyst bed was used to monitor the temperature. The effluent gases were analyzed on-line by a mass spectrometer (HP G-1800A). The sample was pretreated in O_2 (30 ml min^{-1}) at a desired temperature for 1 h and purged with He (30 ml min^{-1}) for 0.5 h before the test.

The $^{18}O/^{16}O$ isotope exchange and CO oxidation by lattice oxygen were employed to investigate the mobility of lattice oxygen in the solid solutions. A sample (0.2 g) was placed in a micro-reactor and was thermally treated in He (HKO, >99.995%, 20 ml min^{-1}) at a desired temperature for 0.5 h. Then $^{18}O_2$ (HKO, 95−98%) was pulsed onto the sample (He as carrier gas, 20 ml min^{-1}) at various temperatures and the composition of the outlet gas was monitored by a mass spectrometer. The data were taken at the 10th pulse where the reaction reached a steady state.

The crystal structure of the catalyst was determined on an X-ray diffractometer (D−MAX, Rigaku) operating at 40 kV and 200 mA using Cu Kα radiation. The patterns recorded were referred to the powder diffraction files—1998 ICDD PDF Database for the identification of crystal structures. The specific surface area of a catalyst was measured using the BET method on a Nova 1200 apparatus.

XPS (Phi Quantum 2000) technique was used to determine the core-level binding energies of the anions and cations in the samples, using monochromatic Al Kα as the excitation source. After oxidation in O_2 at 500 °C or reduction in 5% H_2−95% N_2 at 650 °C, followed by He purging for 10 min, a sample was transferred to a sample holder without being exposed to air in a transparent Glove Bag (Instruments for Research and Industry, USA) filled with He. Finally, the samples were outgassed in vacuum (10^{-5} Torr) for 0.5 h and then introduced into the analyzer chamber (3×10^{-9} Torr) for analysis. The C 1s line at 284.6 eV was taken as a reference for binding energy (BE) calibration.

3. Results and discussion

3.1. Surface morphology and defective structure

The textural properties and surface composition of the CZ, PZ, CZY, PZY, 0.5 wt.% M/CZY, and 0.5 wt.% M/PZY (M = Rh, Pt, Pd) samples are summarized in Table 1. The surface areas of CZ and PZ are 52.9 and 9.80 $m^2\,g^{-1}$. As Y^{3+} ions were incorporated into the CZ and PZ lattices, resulting in the generation of CZY and PZY solid solutions, the specific surface area increased to 69.1 $m^2\,g^{-1}$ for CZY and 54.1 $m^2\,g^{-1}$ for PZY, respectively. The doping of 0.5 wt.% noble metal on the CZY and PZY resulted a slight decrease in specific surface area. The Ce/Zr and Pr/Zr atomic ratios (based on XPS results) of CZ and PZ were 0.34 and 0.69, respectively. They are smaller than the theory ratio of 1.5 (if the distributions of RE and Zr are same on the surface and in the bulk), suggesting that the enrichment of Zr on the surface occurred. When Y^{3+} ions were introduced into the CZ and PZ lattices, Ce/Zr atomic ratio increased to 0.78, whereas Pr/Zr atomic ratio increased to 1.82, indicating that the Zr accumulation on the surface was suppressed and Pr element was enriched on the PZY surface. The average pore diameters of CZ (63.5 Å) and CZY (48.7 Å) were smaller than those of PZ (117 Å) and PZY (61.9 Å),

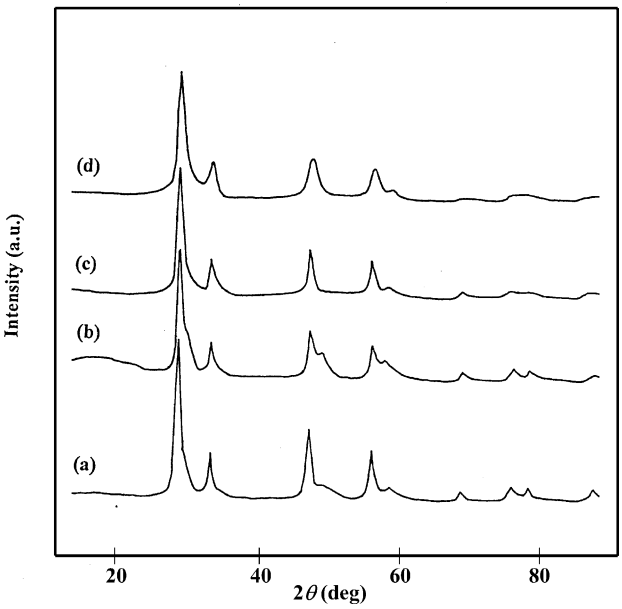

Fig. 1. XRD profiles of fresh: (a) CZ; (b) CZY; (c) PZ; and (d) PZY samples.

respectively. The total pore volume was 0.0671 ml g^{-1} for CZ, 0.0292 ml g^{-1} for PZ, 0.0643 ml g^{-1} for CZY, and 0.0810 ml g^{-1} for PZY. When the 0.5 wt.% noble metal was supported on the CZY and PZY, the Ce(Pr)/Zr atomic ratio and pore volume remained unsignificant changes.

X-ray diffraction investigations on the fresh samples revealed that there were two cubic phases ($Ce_{0.75}Zr_{0.25}O_2$, major; $ZrO_{1.87}$, minor) in CZ and CZY, but only one cubic phase in PZ and PZY (Fig. 1). Based on line-broadening analysis (Table 1), the average particle sizes of CZ and PZ were estimated to be 7.50 and 10.0 nm, respectively; the inclusion of Y^{3+} ions in the CZ and PZ lattices caused the average particle sizes to reduce to 6.62 and 4.16 nm. In other words, the particle size of CZ was smaller than that of PZ, whereas that of CZY was larger than that of PZY. After TPR treatments, no significant changes were observed on

Table 1
Surface area (*S*), average pore diameter (*D*), total pore volume (*V*), average particle size[a] (*P*), surface composition, and Ce(Pr)/Zr atomic ratio

Catalyst	*S* ($m^2\,g^{-1}$)	*D* (Å)	*V* (ml g^{-1})	*P* (nm)	Surface composition (mol%)							Atomic ratio
					Pd	Pt	Rh	Ce/pr	Zr	Y	O	Ce(Pr)/Zr
CZ	52.9	63.5	0.0671	7.50	–	–	–	5.02	14.6	–	80.3	0.34
CZY	69.1	48.7	0.0643	6.62	–	–	–	6.55	8.38	2.44	82.6	0.78
PZ	9.8	117	0.0292	10.0	–	–	–	5.95	9.31	–	84.7	0.69
PZY	54.1	61.9	0.0810	4.16	–	–	–	6.02	3.31	4.36	86.3	1.82
0.5 wt.% Pd/CZY	36.3	59.0	0.0536	14.0	0.13	–	–	5.98	9.30	2.65	81.9	0.64
0.5 wt.% Pt/CZY	37.8	57.9	0.0548	22.5	–	0.64	–	7.12	11.0	4.14	77.1	0.64
0.5 wt.% Rh/CZY	36.9	57.5	0.0531	16.1	–	–	1.98	4.28	6.26	2.75	84.7	0.68
0.5 wt.% Pd/PZY	50.3	67.8	0.0654	6.25	0.34	–	–	6.78	3.97	4.45	84.6	1.70
0.5 wt.% Pt/PZY	51.9	68.9	0.0765	5.62	–	0.67	–	7.10	4.07	4.78	82.7	1.74
0.5 wt.% Rh/PZY	50.7	65.7	0.0740	4.32	–	–	1.78	6.08	4.56	4.34	83.2	1.33

[a] Estimated according to the method of XRD line-broadening.

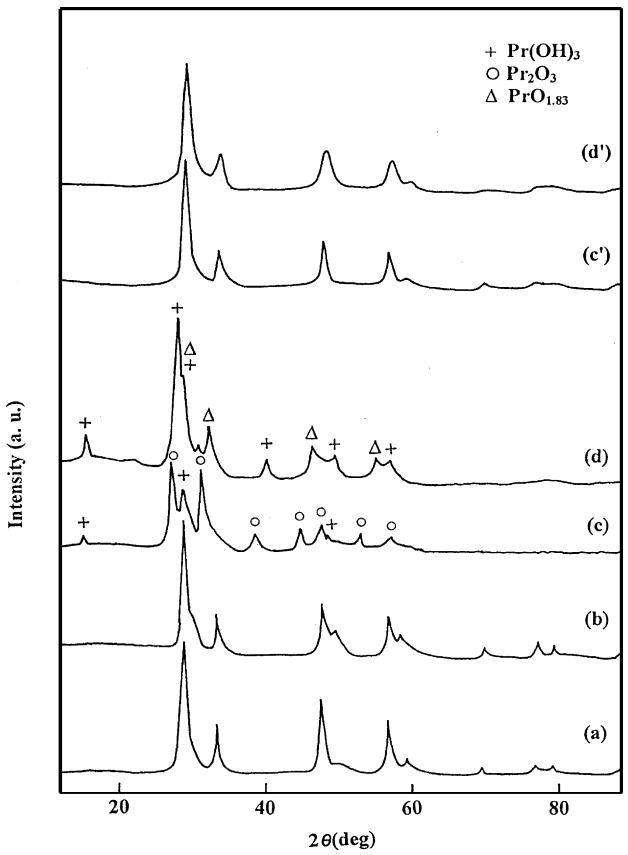

Fig. 2. XRD profiles of reduced: (a) CZ; (b) CZY; (c) PZ; and (d) PZY as well as reoxidized (at 500 °C in O_2 for 2 h) (c′) PZ and (d′) PZY samples.

the XRD patterns of CZ and CZY (Fig. 2a and b) and the remarkable changes (Fig. 2c and d) were found on PZ and PZY. There were two new phases—hexagonal $Pr(OH)_3$ and hexagonal Pr_2O_3 in the reduced PZ sample, and hexagonal $Pr(OH)_3$ and cubic $PrO_{1.83}$ in the reduced PZY sample. By treating the reduced PZ and PZY samples (those after TPR experiments) in O_2 at 500 °C for 2 h, one could revert the samples to their original structures (Fig. 2c′ and d′).

It is well known that the crystal structure of a CeO_2-ZrO_2 solid solution is dependent on chemical composition and synthesis procedure. Tani et al. [26] and Duran et al. [27] reported that below 1000 °C, phase diagram of CeO_2-ZrO_2 shows a single-phase region of a monoclinic structure with a CeO_2 content <20 mol% and only one cubic phase above a CeO_2 content of 80 mol%, while two metasable tetragonal phases (t', t'') were detected at intermediate compositions [22]. As suggested by Vidmar et al. [8] the stable t phase is formed via the decomposition of a diffusional phase, the metastable t' phase is generated via a diffusionless transition, and the t'' phase is an intermediate between the t' and c phases. Up to now, it is a general accepted that the presence of a single-phase solid solution is preferable compared to microdomain or non-homogeneous CeO_2–ZrO_2 mixed oxides, because the former generally lead to better textural stability and redox properties [28,29]. As for the CZ and CZY samples (in which the CeO_2 contents are in the 20−80 mol% range) in this study, two c phases ($Ce_{0.75}Zr_{0.25}O_2$ and $ZrO_{1.87}$) were detected as shown in Fig. 1a and b. It indicated that under the conditions adopted in our work for Ce−Zr−O preparation, there was a phase separation: the excessive amount of Zr existed as $ZrO_{1.87}$ and the solid solution turned out to be $Ce_{0.75}Zr_{0.25}O_2$. For the PZ and PZY solid solutions, however, there was only one cubic phase. It demonstrated that, compared to CeO_2, PrO_2 exhibited a higher ability in dissolving ZrO_2. Although there were hexagonal $Pr(OH)_3$ and Pr_2O_3 phases in PZ and hexagonal $Pr(OH)_3$ and cubic $PrO_{1.83}$ phases in PZY after TPR studies, the original PZ and PZY cubic phases could be completely restored by means of reoxidation in O_2 at 500 °C for 2 h (Fig. 2c′ and d′). In other words, PZ and PZY display a reversible reduction/oxidation character. The formation of a CZY or PZY solid solution by doping Y^{3+} and Zr^{4+} ions into a CeO_2 or PrO_2 lattice would generate even more oxygen vacancies and/or RE^{3+} ions due to charge balance requirement, resulting in a promotion in the redox properties and oxygen storage capacity.

3.2. Oxygen storage capacity, oxygen mobility, and redox properties

The oxygen storage capacity and redox properties of the samples employed in this work were investigated by TPR, O_2-TPD, as well as O_2–H_2 and O_2–CO titration methods. The TPR profiles of CZ, CZY, PZ, and PZY are illustrated in Fig. 3. For CZ, a sharp reduction band at ca. 570 °C with

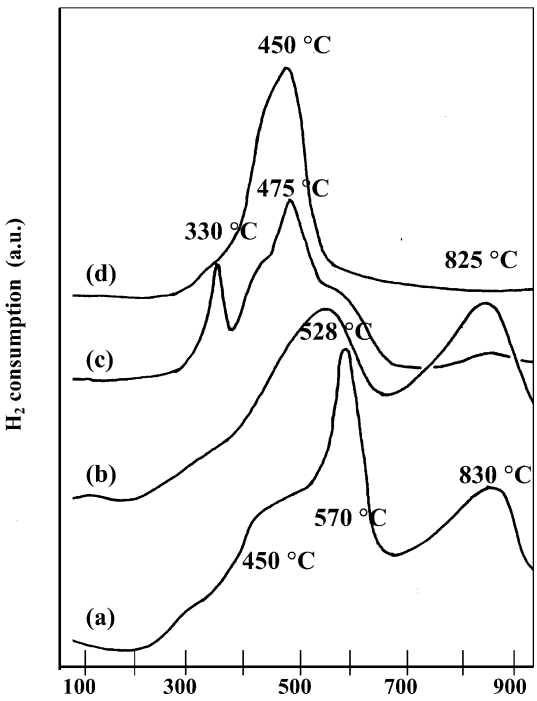

Fig. 3. TPR profiles of: (a) CZ; (b) CZY; (c) PZ; and (d) PZY samples.

a shoulder at ca. 450 °C and a broad band at ca. 830 °C were observed, indicating that there are at least two types of Ce^{4+} located at different chemical environments. The reduction bands at 450 and 570 °C could be assigned to the reduction of surface and subsurface Ce^{4+}, whereas the band at 830 °C to the reduction of bulk Ce^{4+}. For CZY, there were two reduction bands at ca. 528 and 825 °C due to the reduction of Ce^{4+} located on the surface (subsurface) and in bulk, respectively. There were two big reduction bands at ca. 330 and 475 °C with two shoulders at ca. 420 and 570 °C over PZ and only one big band was observed at 450 °C over PZY, suggesting that the reduction of Pr^{4+} sited in the bulk occurred, together with the reduction of Pr^{4+} on surface, at lower temperature compared to the Ce-based samples. The amounts of reducible oxygen of the samples were 0.997, 0.960, 1.43, 1.59 mmol g^{-1}, for CZ, CZY, PZ, and PZY, respectively, based on calculation of H_2 consumption during the TPR experiments.

Fig. 4 illustrates the O_2-TPD profiles of CZ, CZY, PZ, and PZY. Three desorption peaks at ca. 490, 655, and 870 °C were observed over CZ (Fig. 4a). The extent of O_2 desorption corresponding to the first peak was 3.4×10^{-3} mmol g^{-1} and that corresponding to the other two small peaks was 1.1×10^{-3} mmol g^{-1}. With Y^{3+} incorporation into the lattice of CZ, there were a large peak (extent of O_2 desorption, 2.5×10^{-2} mmol g^{-1}) at ca. 570 °C and a shoulder peak at ca. 490 °C; the third one remained almost unchanged (Fig. 4b). For PZ (Fig. 4c), a sharp peak at ca. 405 °C and a broad one at ca. 675 °C were observed; the amounts of O_2 desorption were 3.7×10^{-3} and 1.3×10^{-1} mmol g^{-1}, respectively. For PZY (Fig. 4d), there were three peaks at ca. 415, 675, and 870 °C; the corresponding O_2 desorption were 1.0×10^{-1}, 2.4×10^{-2} and 1.4×10^{-2} mmol g^{-1}.

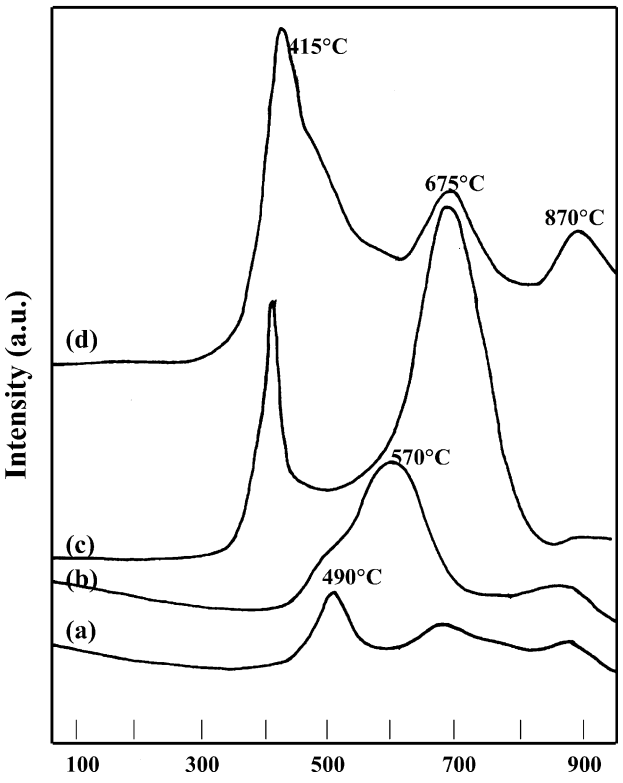

Fig. 4. O_2-TPD profiles of: (a) CZ; (b) CZY; (c) PZ; and (d) PZY.

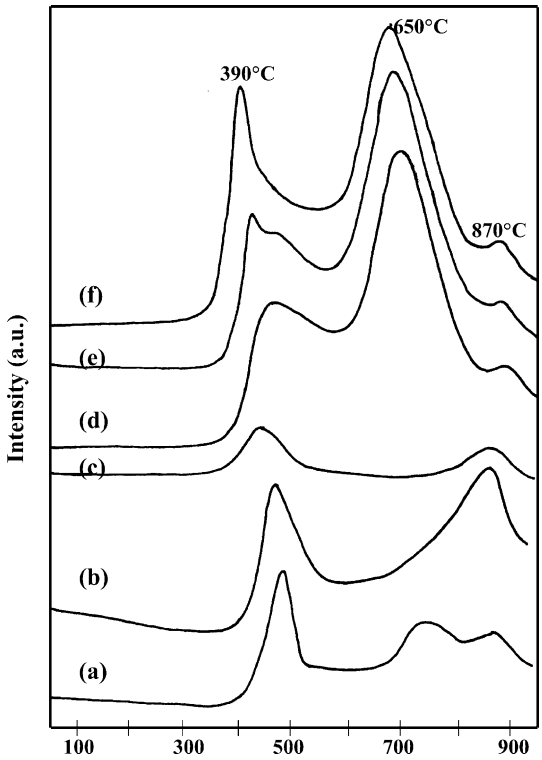

Fig. 5. O_2-TPD profiles of: (a) 0.5 wt.% Pd/CZY; (b) 0.5wt% Pt/CZY; (c) 0.5 wt.% Rh/CZY; (d) 0.5 wt.% Pd/PZY; (e) 0.5 wt.% Pt/PZY; (f) 0.5 wt.% Rh/PZY samples.

The O_2-TPD profiles of 0.5 wt.% M/CZY and 0.5 wt% M/PZY (M = Rh, Pt, and Pd) were shown on the Fig. 5. Two O_2 desorption peaks at ca. 430 and 860 °C were observed on the 0.5 wt.% M/CZY samples. Compared to O_2-TPD profile of CZY, one can see that the doping of noble metal on CZY caused a shift of the first O_2 desorption peak to lower temperature, whereas the O_2 desorption at around 860 °C remained unchanged. As for 0.5 wt.% M/PZY samples, there were three O_2 desorption peaks observed at near to 400, 660, and 850 °C. Like in the case of 0.5 wt.% M/CZY, when the 0.5 wt.% noble metals were loaded on the PZY solid solution, the first O_2 desorption peak shifted to lower temperature. The significant changes of the O_2 desorption amount at ca. 660 °C were exhibited on the O_2-TPD profiles of 0.5 wt.% M/PZY samples, indicating that the presence of noble metal can promoted the heating reduction in bulk for PZY solid solution.

The O_2-H_2 and O_2-CO titration experiments were conducted to study the redox behavior and oxygen storage ability of the samples and the results are summarized in Table 2. It can be observed that the O_2 uptakes as measured in O_2-H_2 and O_2-CO titrations as well as the O_2 uptakes calculated

Table 2
Oxygen uptake as measured by O_2-H_2 and O_2-CO titration at 450 °C

Sample	O_2 uptake[a] (mmol g^{-1})			
	O_2-H_2 titration	O_2-CO titration		
	A	A	B	C
CZ	0.36	0.31	0.36	0.32
CZY	0.54	0.5	0.52	0.5
PZ	0.40	0.37	0.38	0.34
PZY	0.75	0.71	0.69	0.72

[a] An average of three cycles. (A) Result based on O_2 consumption; (B) result based on CO consumption in CO pulsing; (C) result based on CO_2 production in CO pulsing.

according to the amounts of CO consumed and CO_2 produced in the O_2-CO titration were roughly the same, indicating that the data are reliable. In the three consecutive cycles of the O_2-H_2 or O_2-CO titration, the O_2 uptakes estimated according to O_2 consumption were similar, suggesting that the redox behavior is reversible. The oxygen uptakes of CZ, CZY, PZ, and PZY were ca. 0.3, 0.5, 0.4, and 0.7 mmol g^{-1}, respectively, showing that Y^{3+} incorporation increased the O_2 uptake ability of CZ and PZ. One can observe that PZ and PZY are superior to CZ and CZY, respectively, in oxygen uptake in the redox cycles.

In a summary, based on the extent of oxygen uptake (Table 2), one can see that the ability of storing oxygen followed a sequence of PZY > CZY > PZ > CZ, coinciding with the order of the oxygen vacancy density. The process for oxygen uptake involves a redox cycle between RE^{4+} and RE^{3+} (RE = Ce, Pr) and the oxygen vacancies generated by Y^{3+} incorporation facilitate the reduction of RE^{4+} to RE^{3+}. The reducibility of the materials followed an order of PZY > PZ > CZY ≈ CZ, similar to the sequence of the amounts of desorbable oxygen (O_2-TPD results).

The $^{18}O/^{16}O$ isotope exchange experiments were performed in order to probe the oxygen mobility of the solid solutions and the results are shown in Figs. 6 and 7. The take-off temperatures for exchanges were markedly different for the Ce- and Pr-based solid solutions: they were 350 and 450 °C over the Ce- and Pr-based samples, respectively. The extent of $^{18}O/^{16}O$ exchange increased with temperature rise. For the CZ sample, the concentrations of $^{18}O_2$, $^{16}O_2$, and $^{18}O^{16}O$ were 82, 17, 1.0%, respectively, at 550 °C (Fig. 6a). With the incorporation of Y^{3+}, $^{18}O^{16}O$ exchange became significant; 61% $^{18}O_2$, 20% $^{16}O_2$, and 19% $^{18}O^{16}O$ were detected over CZY at 550 °C (Fig. 6b). For the PZ sample, the concentrations of $^{18}O_2$, $^{16}O_2$, and $^{18}O^{16}O$ were 19, 70, 11%, respectively, at 550 °C (Fig. 6c). The incorporation of Y^{3+} into the PZ lattice enhanced $^{18}O^{16}O$ exchange considerably; 0% $^{18}O_2$, 76% $^{16}O_2$, and 24% $^{18}O^{16}O$ were observed over PZY at 550 °C (Fig. 6b).

As 0.5 wt.% Pt or 0.5 wt.% Pd was doped onto the CZY and PZY samples, the take-off temperatures for $^{18}O/^{16}O$ isotope exchange decreased ca. 50 °C (Fig. 7). For 0.5 wt.% Rh/CZY and 0.5 wt.% Rh/PZY samples, the take-off temperatures of the exchange were not observed to have a significant change. But the extent of $^{18}O/^{16}O$ isotope exchange at 550 °C increased by doping Rh, Pt, and Pd on CZY and PZY samples: the concentrations of exchange product ($^{16}O_2$) at 550 °C were 49.6, 38.0, 20.2, 84.7, 86.7, and 87.7%, respectively, over 0.5 wt.% Rh/CZY, 0.5 wt.% Rt/CZY, 0.5 wt.% Rt/CZY, 0.5 wt.% Rh/PZY, 0.5 wt.% Rt/PZY, and 0.5 wt.% Rt/PZY samples.

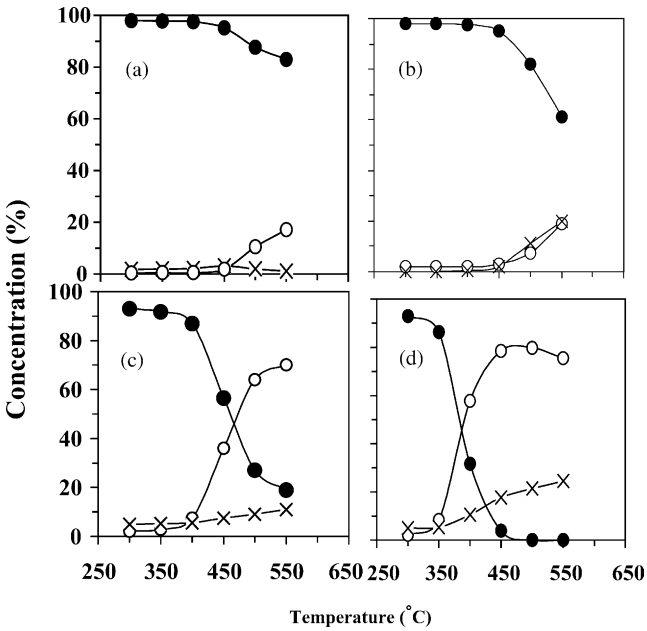

Fig. 6. $^{18}O-^{16}O$ isotopic exchange over (a) CZ, (b) CZY, (c) PZ, (d) PZY: (●) $^{18}O_2$; (○) $^{16}O_2$; (×) $^{18}O^{16}O$ concentrations.

Oxygen mobility is an important factor to consider what solid oxides can be used as catalysts in the oxidation of carbon monoxide and hydrocarbons [30] as well as in the removal of automotive exhaust [31]. As proposed by Novakova and co-workers [32,33], $^{18}O-^{16}O$ interactions over an oxide surface could proceed according to the three pathways: (i) homoexchange in the gas phase without appreciable participation of oxygen in the oxide (Eq. (1)); (ii) single heteroexchange with the involvement of only one oxygen from the oxide surface (Eqs. (2) and (3)); and (iii) multiple heteroexchange with the participation of two surface oxygen atoms from the oxide (Eqs. (4)–(6)).

$$^{18}O_{2(g)} + {}^{16}O_{2(g)} \Leftrightarrow 2\,{}^{18}O^{16}O_{(g)} \quad (1)$$

$$^{18}O^{18}O_{(g)} + {}^{16}O_{(S)} \Leftrightarrow {}^{18}O^{16}O_{(g)} + {}^{18}O_{(s)} \quad (2)$$

$$^{18}O^{16}O_{(g)} + {}^{16}O_{(s)} \Leftrightarrow {}^{16}O^{16}O_{(g)} + {}^{18}O_{(s)} \quad (3)$$

$$^{18}O^{18}O_{(g)} + 2\,{}^{16}O_{(s)} \Leftrightarrow {}^{16}O_{2(g)} + 2\,{}^{18}O_{(s)} \quad (4)$$

$$^{18}O^{16}O_{(g)} + 2\,{}^{16}O_{(s)} \Leftrightarrow {}^{16}O_{2(g)} + {}^{16}O_{(s)} + {}^{18}O_{(s)} \quad (5)$$

$$^{18}O^{16}O_{(g)} + 2\,{}^{18}O_{(s)} \Leftrightarrow +{}^{18}O_{2(g)} + {}^{16}O_{(s)} + {}^{18}O_{(s)} \quad (6)$$

It has been suggested that there are two possible mechanisms for multiple heteroexchange [34–36]: one is isotope

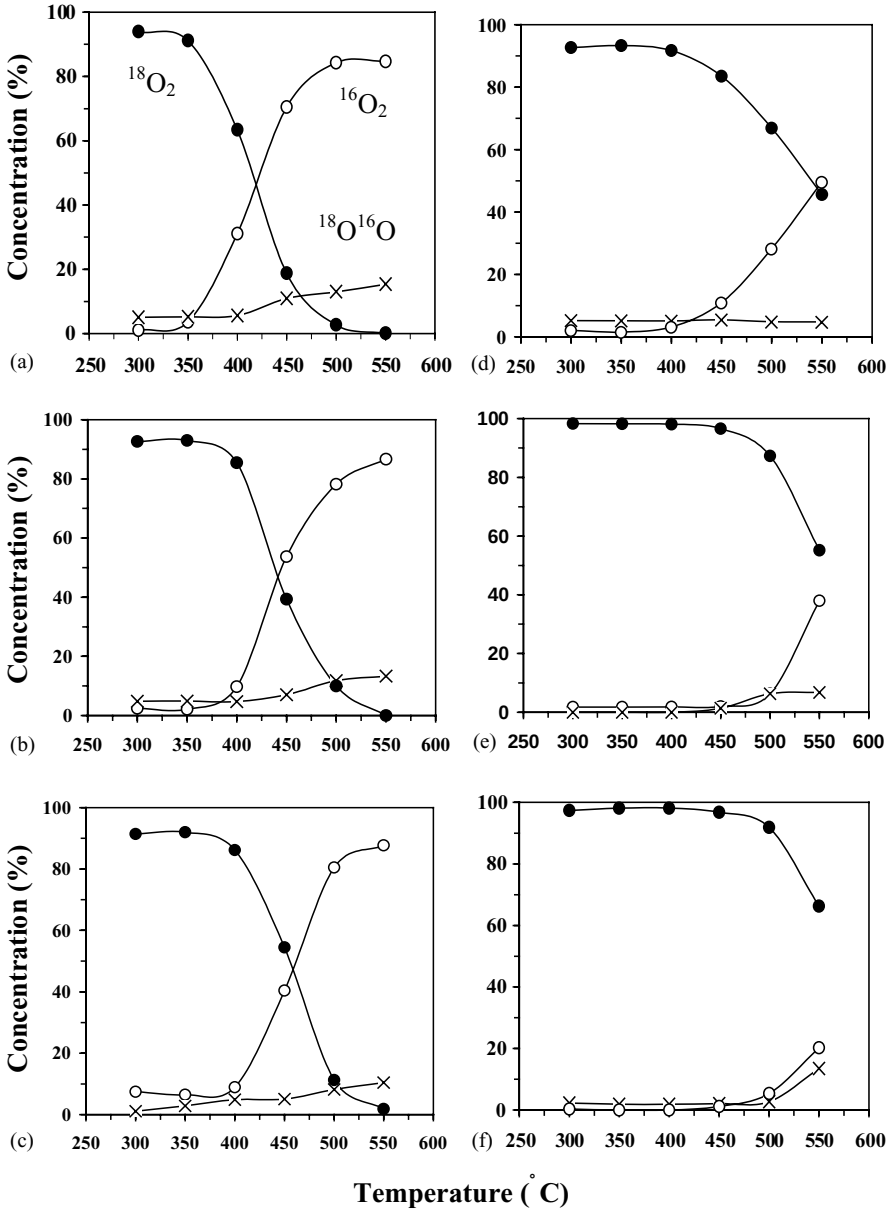

Fig. 7. ^{18}O–^{16}O isotopic exchange over 0.5 wt.% Rh/PZY (a), 0.5 wt.% Pt/ PZY (b), 0.5 wt.% Pd/PZY (c), 0.5 wt.% Rh/CZY (d), 0.5 wt.% Pt/CZY (e), and 0.5 wt.% Pd/CZY (f): (●) $^{18}O_2$; (○) $^{16}O_2$; (×) $^{18}O^{16}O$ concentrations.

exchange via a four-atom surface intermediate [$(O_4)^-_{ads}$] and the other is "place-exchange" via the displacement of a preadsorbed oxygen molecule by an oxygen molecule from the gas phase. As shown in Fig. 6, the $^{18}O^{16}O$ concentrations at 550 °C were ca. 1, 19, 11, and 24%, respectively, over CZ, CZY, PZ, and PZY, implying that the exchange in gas phase was negligible. The logic is that if the exchange in the gas phase was dominant, the $^{18}O^{16}O$ concentration should be similar over the four samples. Martin and Duprez [31] detected roughly equal fractions of $^{18}O^{16}O$ and $^{16}O_2$ during $^{18}O/^{16}O$ exchanges over H_2-reduced CeO_2 and suggested that exchange took place equally via the single (Eqs. (2) and (3)) and multiple (Eqs. (4)–(6)) heteroexchange mechanisms. Oxygen isotope exchanges proceeded at or above 450 °C over CZ and CZY. Over PZ and PZY, however, the exchanges occurred at a lower temperature and in a bigger extent above 400 and 350 °C, respectively. These results indicate that: (i) the activity of lattice oxygen in Pr-based solid solutions was higher than that in Ce-based solid solutions; and (ii) the inclusion of Y^{3+} in a CZ or PZ lattice enhanced the activity of lattice oxygen. Generally speaking, there are several oxygen adspecies such as O_2^-, O_2^{2-}, and O^- on the surface of an oxygen-containing catalyst. By using the technique of electron paramagnetic resonance, Martínez-Arias et al. [37] detected O_2^-–Zr^{4+} and O_2^-–Ce^{4+} on $Ce_{0.5}Zr_{0.5}O_2$. These oxygen species can intertransform via a sequence of $O_2^- \Leftrightarrow O_2^{2-} \Leftrightarrow O^- \Leftrightarrow O^{2-}_{lattice}$ at elevated temperatures. According to Seiyama [38]

and Zhang et al. [39], O_2 adsorbed dissociatively to form O^- species at oxygen vacancies on a perovskite-type oxide. Similarly, O_2 adsorption and O^- generation are expected to occur at the V_o positions of CZ, CZY, PZ, and PZY. An O^- could pick up one more electron to become $O^{2-}{}_{lattice}$. On the basis of the fact that the concentrations of $^{18}O^{16}O$ and $^{16}O_2$ detected over CZY (Fig. 6b) are rather close, one can deduce that the $^{18}O/^{16}O$ exchanges over CZY proceed mainly via both the single (Eqs. (2) and (3)) and multiple (Eqs. (4)–(6)) heteroexchange mechanisms, just as in the case of H_2-reduced CeO_2 [31]. Above 400 °C over PZ and above 350 °C over PZY, the concentration of $^{16}O_2$ was much higher than that of $^{18}O^{16}O$, implying that $^{18}O/^{16}O$ exchanges proceeded mainly via the multiple heteroexchange mechanism (Eqs. (4)–(6)). This is reasonable because the amount of oxygen vacancies that are available in PZ and PZY are higher than that of CZ and CZY. It is apparent that the incorporation of Y^{3+} into CZ and PZ increased the V_o concentration (as reflected in the enhanced amount of O_2 desorption over CZY (Fig. 4b) and PZY (Fig. 4d)), resulting in an enhancement in $^{18}O/^{16}O$ exchange. Compared to that of PZ, the Pr^{4+} content in Y^{3+}-doped PZ was higher, indicating that there were more oxygen vacancies in PZY than in CZY at $x = 0.05$. It is well known that oxygen mobility in a solid oxide increases with an increase in V_o concentration. Since the amount of oxygen vacancies in CZ is smaller than that in CZY, PZ or PZY, oxygen isotope exchange over CZ would preferentially follow the "place-exchange" mechanism. The fact that the amount of $^{16}O_2$ is higher than that of $^{18}O^{16}O$ over CZ (Fig. 6a) supports this viewpoint.

3.3. CO oxidation by lattice oxygen

In order to understand the lattice oxygen activities of the two kinds of solid solutions, we used CO as a probe. Before performing the CO-pulsing experiments, a sample was heated in He at 500 °C for 1 h to guarantee a complete removal of oxygen adspecies on the surface of the sample. The results collected within a temperature range of 200–450 °C are illustrated in Fig. 8. The conversion of CO over PZ was slightly higher than that over CZ. Comparing to CZ and PZ, CO conversion over CZY and PZY was significantly higher. Below 350 °C, CO conversion over PZY was similar to that over CZY; above 350 °C the former was much higher than the latter. At 450 °C, CO conversions were 32.9, 46.3, 40.0, and 70.1% over CZ, CZY, PZ, and PZY, respectively. The results indicate that: (i) the doping of Y^{3+} into the lattices of CZ and PZ enhanced the activity of lattice oxygen; and (ii) lattice oxygen in PZ and PZY showed a high oxidation activity than that in CZ and CZY, respectively.

3.4. XPS studies

Fig. 9 shows the Ce 3d spectra of the CZ and CZY samples treated in O_2 at 500 °C and H_2 at 650 °C. It is observed that there were two sets of spin-orbit multiplets: u and v

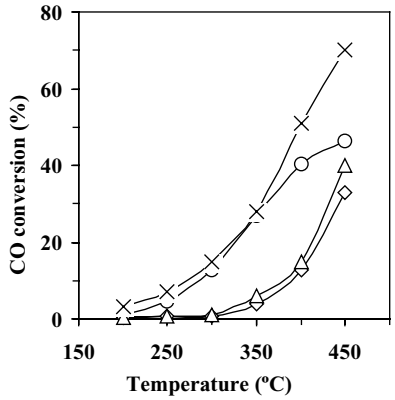

Fig. 8. CO oxidation in pulse reaction over the CZ (◇), CZY (○), PZ (△), and PZY (×) samples.

correspond to $3d_{3/2}$ and $3d_{5/2}$ contributions, respectively; the Ce 3d spectrum contains three main $3d_{5/2}$ features at ca. 882.5 (v), 889.4 (v_2), and 898.7 (v_3) eV and three main $3d_{3/2}$ features at ca. 900.6 (u), 907.7 (u_2), and 916.6 (u_3) eV; u_3 and v_3 could be assigned to the $3d^9\ 4f^0$ photoemission final state, whereas the (v, v_2) and (u, u_2) doublets could be attributed to final states with a strong mixing of the $3d^9\ 4f^2$ and $3d^9\ 4f^1$ configurations. These states arise from the core hole potential in the final state and 4f hybridization in the initial state [40–43]. The v and v_2 as well as u and u_2 features are shake-down signals due to charge transfer from ligand (O 2p) to metal (Ce 4f). According to the assignment convention proposed by Burroughs et al. [44], the states at 885.6 eV (v_1) and 903.9 eV (u_1) belong to unique photoelectron features from the Ce^{3+} state and the states at 907.7 eV can be assigned to Ce^{4+}. From Fig. 9, it can be observed

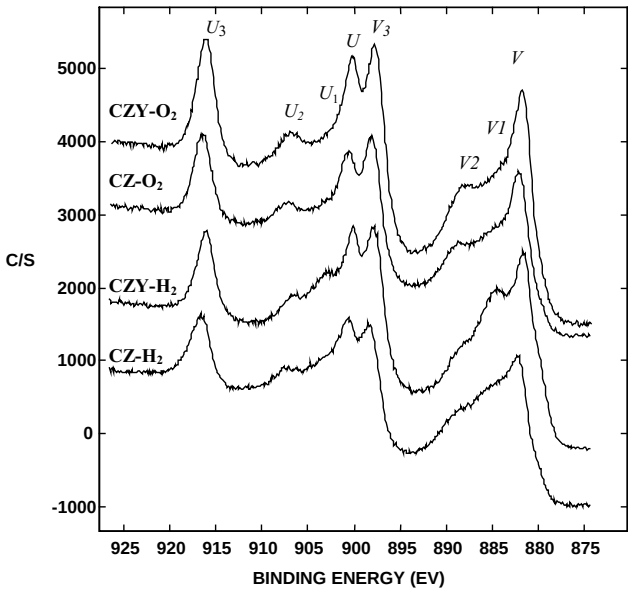

Fig. 9. Ce 3d spectra of CZ and CZY samples treated: in O_2 at 500 °C (CZ–O_2 and CZY–O_2); in H_2 at 650 °C (CZ–H_2 and CZY–H_2).

that: (i) the peaks at 885.6 eV and 903.9 eV are displayed on the Ce 3d spectra of reduced CZ and CZY samples (Fig. 9 (CZ-H_2 and CZY-H_2)), whereas they disappear for the oxidized CZ and CZY samples, indicating that the amount of Ce^{3+} ions decreased in O_2 treatment, but increased in H_2 treatment; (ii) the intensity of the peak at 907.7 eV decrease in the order of CZY–O_2 > CZ–O_2 > CZY–H_2 ≈ CZ–H_2, suggesting that the amount of Ce^{4+} ions increased in O_2 treatment, but decreased in H_2 treatment and the more Ce^{4+} ions can be determined on CZY sample than these on CZ samples in the oxidative condition. In addition, one can also see that the intensities of Ce^{3+} ions signals on CZY-H_2 spectrum are higher than that on CZ-H_2 spectrum, suggesting the more Ce^{3+} ions existed on CZY sample compared to CZ samples in the reductive condition.

Similar things occurred for the PZ and PZY samples. The Pr 3d spectra of PZ and PZY treated in H_2 and O_2, respectively, are Shown in Fig. 10. Two sets of spin-orbit multiples are observed at binding energies of ca. 953.5 and 933.9 eV, which represent the $3d_{3/2}$ and $3d_{5/2}$ of Pr, respectively. According to the results of Narula et al. [25], Matsumura et al. [45], Sarma and Rao [46], we assign the signals at ca. 933.9, 953.5, and 966.4 eV to Pr^{4+} and the signals at ca. 929.5, 949.8, and 973.2 eV to Pr^{3+}. The satellites are due to the spin-orbit splitting. After O_2-treatment, the content of Pr^{4+} over PZY was larger than over PZ, whereas the more Pr^{3+} ions were examined on PZY than on PZ sample in reductive condition.

From the results of Ce 3d and Pr 3d spectra studies, we can gain a conclusion that the introduction of Y^{3+} into CZ and PZ solid solutions is beneficial for the $RE^{4+} \Leftrightarrow RE^{3+}$ redox process, i.e. the reducible-reoxidizable Ce^{n+} or Pr^{n+} ions are increased by the presence of Y^{3+} in the condition employed in this work.

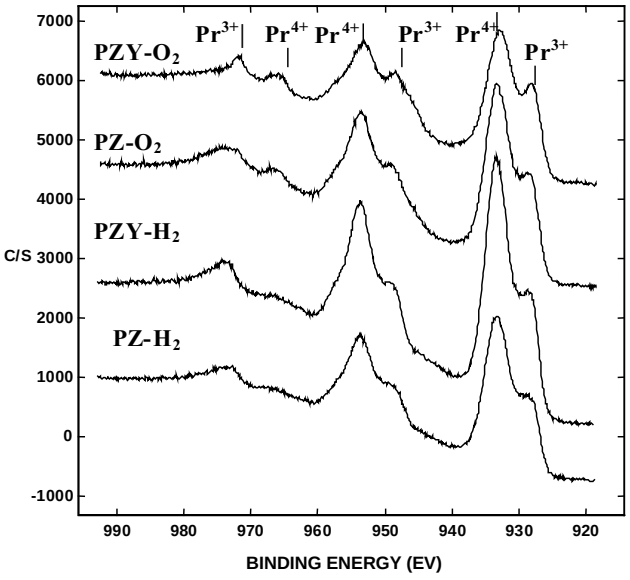

Fig. 10. Pr 3d spectra of PZ and PZY samples treated: in O_2 at 500 °C (PZ–O_2 and PZY–O_2); in H_2 at 650 °C (PZ–H_2 and PZY–H_2).

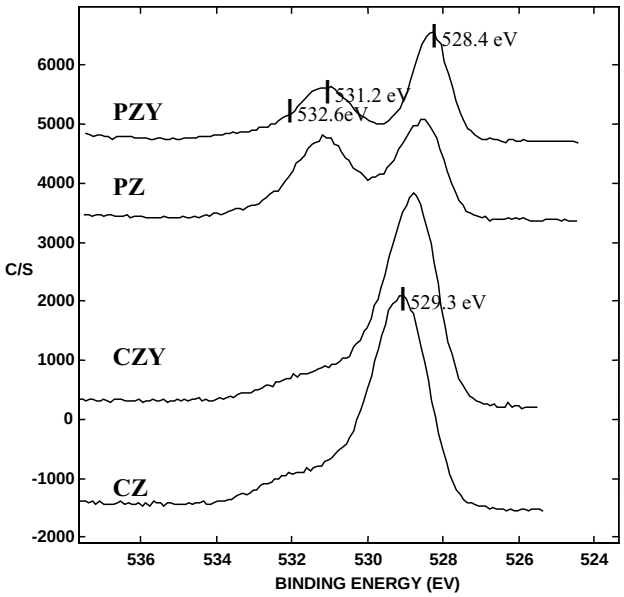

Fig. 11. O1s spectra of CZ, CZY, PZ, and PZY samples treated in O_2 at 500 °C.

The O1s spectra for the CZ, CZY, PZ, and PZY samples, treated in O_2 before the test, are presented in Fig. 11. Three different oxygen components can be found at ca. 529 (shift from 529.4 to 528.4 eV in the sequence of CZ, CZY, PZ, and PZY), 531.2, and 532.6 eV. The former one can be assigned to lattice O^{2-} and the later two is due to the presence of adsorptive O_2 or/and weekly bonded oxygen species. The intensities of O1s signals at 531.2 and 532.6 eV over Pr-based solid solution are much higher than over Ce-based samples, implying the higher activity of surface oxygen on Pr-based samples than Ce-based materials. It is coincide with the results of O_2-TPD, TPR, and $^{18}O/^{16}O$ isotope exchange experiments.

4. Conclusion

The CZ, CZY, PZ, and PZY solid solutions existed as nano-particles and the addition of yttrium caused a reduction in the particle sizes of CZ and PZ. There were cubic $Ce_{0.75}Zr_{0.25}O_2$ (major) and $ZrO_{1.87}$ (minor) phases in CZ and CZY, whereas in PZ and PZY there was only one cubic phase. The results of TPR and O_2-TPD revealed that the redox action of $Pr^{4+} \Leftrightarrow Pr^{3+}$ occurred at lower temperature than the $Ce^{4+} \Leftrightarrow Ce^{3+}$ redox process and presence of Y^{3+} facilitated the redox process. Results of H_2 (or CO)−O_2 titration revealed that redox of Ce^{4+}/Ce^{3+} or Pr^{4+}/Pr^{3+} was reversible and oxygen storage capacity followed a sequence of PZY > CZY > PZ > CZ. The outcome of $^{18}O/^{16}O$ exchange confirmed the promotional effects of oxygen vacancies on the mobility of lattice oxygen. The results of XPS studies illustrated that the introduction of Y^{3+} into CZ and PZ solid solutions was beneficial for the $RE^{4+} \Leftrightarrow RE^{3+}$

redox process, i.e. the amount of reducible-reoxidizable Ce^{n+} or Pr^{n+} ions was increased by the existence of Y^{3+} in the conditions employed in this work. We conclude that: (i) a Pr-based solid solution has better redox behavior than a Ce-based one; (ii) incorporation of yttrium ions in the lattices of CZ and PZ solid solutions could result in an enhancement in oxygen vacancy concentration, Ce^{4+}/Ce^{3+} and Pr^{4+}/Pr^{3+} redox properties, lattice oxygen mobility, and oxygen storage capacity; and (iii) doping the noble metal (Rh, Pt, and Pd) onto RE-based solid solution has positive effect on the properties concerned in this work.

References

[1] R.K. Usman, G.W. Graham, W.L.H. Watkins, R.W. McCabe, Catal. Lett. 30 (1995) 53.
[2] A. Bensalem, F. Bozon Verduraz, M. Delamar, G. Bugli, Appl. Catal. A 121 (1995) 81.
[3] F. Zamar, A. Trovarelli, C. De Leitenburg, G. Dolcetti, J. Chem. Soc., Chem. Commun. (1995) 965.
[4] G. Vlaic, R. Di Monte, P. Fornasiero, E.P. Fonda, J. Kašpar, M. Graziani, J. Catal. 183 (1999) 378.
[5] K. Hashimoto, N. Toukai, R. Hamada, S. Imamura, Catal. Lett. 50 (1998) 193.
[6] P. Fornasiero, G.R. Rao, J. Kašpar, F.L. Erario, M. Graziani, J. Catal. 175 (1998) 269.
[7] T. Masui, Y. Peng, K. Machida, G. Adachi, Chem. Mater. 10 (1998) 4005.
[8] P. Vidmar, P. Fornasiero, J. Kašpar, G. Gubitosa, M. Graziani, J. Catal. 171 (1997) 160.
[9] G.R. Rao, P. Fornasiero, R. Di Monte, J. Kašpar, G.G. Vlaic Balducci, S. Meriani, G. Gubitosa, A. Cermona, M. Graziani, J. Catal. 162 (1996) 1.
[10] P. Fornasiero, G. Balducci, R. Di Monte, J. Kašpar, V. Sergo, G. Gubitosa, A. Ferrero, G. Graziani, J. Catal. 164 (1996) 173.
[11] P. Fornasiero, R. Di Monte, G.R. Rao, J. Kašpar, S. Meriani, A. Trovarelli, M. Graziani, J. Catal. 154 (1995) 168.
[12] G.R. Rao, J. Kašpar, S. Meriani, R. Di Monte, M. Graziani, Catal. Lett. 24 (1994) 107.
[13] G. Bulducci, P. Fornasiero, R. Di Monte, J. Kašpar, S. Meriani, M. Graziani, Catal. Lett. 33 (1995) 193.
[14] A. Trovarelli, F. Zamar, J. Llora, C. De Leitenburg, G. Dolcetti, J.T. Kiss, J. Catal. 169 (1997) 490.
[15] C.E. Hori, H. Permana, K.Y. Simon Ng, A. Brenner, K. More, K.M. Rahmoeller, D. Belton, Appl. Catal. B 16 (1998) 105.
[16] Y. Madier, C. Descorme, A.M. Le Govic, D. Duprez, J. Phys. Chem. B 103 (1999) 10999.
[17] A.I. Kozlov, D.H. Kim, A. Yezerets, P. Andersen, H.H. Kung, M.C. Kung, J. Catal. 209 (2002) 417.
[18] L.F. Liotta, A. Macaluso, A. Longo, G. Pantaleo, A. Martorana, G. Deganello, Appl. Catal. A 240 (2003) 295.
[19] M. Boaro, A. Trovarelli, J.H. Hwang, T.O. Mason, Solid State Ionics 147 (2002) 85.
[20] M. Hirano, T. Miwa, M. Inagaki, J. Solid State Chem. 158 (2001) 112.
[21] F. Deganello, A. Martorana, J. Solid State Chem. 163 (2002) 527.
[22] M. Yashima, H. Arashi, M. Kakihana, M. Yoshimura, J. Am. Ceram. Soc. 77 (1994) 1067.
[23] R. Di Monte, P. Fornasiero, M. Graziani, J. Kašpar, J. Alloys Compd. 877 (1998) 275.
[24] H. He, H.X. Dai, L.H. Ng, K.W. Wong, C.T. Au, J. Catal. 206 (2002) 1.
[25] C.K. Narula, L.P. Haack, W. Chun, H.W. Jen, G.W. Graham, J. Phys. Chem. B 103 (1999) 3634.
[26] E. Tani, M. Yoshmura, S. Somiya, J. Am. Ceram. Soc. 66 (1983) 506.
[27] P. Duran, M. Gonalez, C. Moure, J.R. Jurdo, C. Pascal, J. Mater. Sci. 25 (1990) 5001.
[28] J. Kaspar, P. Fornasiero, M. Graziani, Catal. Today 50 (1999) 285.
[29] Y. Sun, P.A. Sermon, J. Mater Chem. 6 (1996) 1025.
[30] L.G. Tejuca, J.L.G. Fierro (Eds.), Properties and Applications of Perovskite-Type Oxides, Dekker, New York, 1993.
[31] D. Martin, D. Duprez, J. Phys. Chem. 100 (1996) 9429.
[32] J. Novakova, Catal. Rev. 4 (1970) 77.
[33] K. Klier, J. Novakova, P. Jiru, J. Catal. 2 (1963) 249.
[34] M. Che, J. Tench, Adv. Catal. 7 (1982) 31;
M. Che, J. Tench, Adv. Catal. 32 (1983) 1.
[35] J. Cunningham, E.L. Goold, J.L.G. Fierro, J. Chem. Soc., Faraday Trans. 78 (1982) 785.
[36] J. Cunningham, D. Cullinane, F. Farrell, J.P. O'Driscoll, M.A.J. Morris, Mater. Chem. 5 (1995) 1027.
[37] A. Martínez-Arias, M. Fernádez-García, C. Belver, J.C. Conesa, J. Soria, Catal. Lett. 65 (2000) 197.
[38] T. Seiyama, in: L.G. Tejuca, J.L.G. Fierro (Eds.), Properties and Applications of Perovskite-Type Oxides, 1993, p. 223.
[39] H.M. Zhang, Y. Shimizu, Y. Teraoka, N. Miura, N. Yamazoe, J. Catal. 121 (1990) 432.
[40] A. Fujimori, Phys. Rev. B 28 (1983) 2282;
A. Fujimori, Phys. Rev. B 53 (1984) 2518.
[41] A. Kotani, H. Mizuta, T. Jo, J.C. Parlebas, Solid State Commun. 53 (1985) 805.
[42] E. Wuilloud, B. Delley, W.-D. Schneider, Y. Baer, Phys. Rev. Lett. 53 (1984) 202;
E. Wuilloud, B. Delley, W.-D. Schneider, Y. Baer, Phys. Rev. Lett. 53 (1984) 2519.
[43] T. Jo, A. Kotani, Phys. Scr. 35 (1987) 570.
[44] P. Burroughs, A. Hamnett, A.F. Orchard, G. Thornton, J. Chem. Soc., Dalton Trans. (1976) 1686.
[45] Y. Matsumura, S. Sugiyama, J.B. Moffat, in: S.T. Oyama, J.W. Hightower (Eds.), Catalytic Selective Oxidation ACS Symp. Ser. ACS, Washington, 1993. p. 326.
[46] D.D. Sarma, C.N.R. Rao, J. Electron Spectrosc. Relat. Phenom. 20 (1980) 25.